Adaptable Wind Tunnel for Testing V/STOL Configurations at High Lift

W.R. Sears*
University of Arizona, Tucson, Arizona

It is argued that the adaptable-wall wind tunnel scheme offers a way to solve a persistent problem of V/STOL testing; namely, interference of tunnel boundaries with the powered, vortical wake at large lift coefficients. First, it is shown that the adaptable-wall scheme permits the simulated freestream direction to be chosen independently of wind tunnel architecture. It is also found that the wake can be allowed to pass downstream without encountering the interface defined by the instrument-array of the tunnel. The combination of these two ideas leads to a new type of wind tunnel—the Arizona V/STOL Tunnel—in which the model's orientation and the freestream vector are chosen to put the wake in the desired position and simulation of the correct freestream vector, defining the desired angle of attack, is achieved by means of the adaptable-wall iterative strategy. To facilitate a numerical demonstration of a tunnel of this kind, a simple panel model of a jet-flap wing and wake is constructed, suitable for the nonlinear, high-lift regime and for the inclusion of wind tunnel effects. Convergence is obtained and the final wing/wake properties are close to unconfined-flow values for the same wing model, although starting conditions were grossly different from preselected final conditions.

Nomenclature

C = jet-momentum coefficient
f,g = flow variables (functions) used to establish unconfined flow in the adaptable-wall scheme
$g[f]$ = the function g according to the computed outer flow determined by boundary values f and the far-field boundary conditions
k = "relaxation factor" defined in Table 1, steps 4 and 6, and Eq. (2)
q = strength of source panel on Σ
S = interface between inner and outer flow regions
u,v,w = Cartesian components in the x,y,z coordinate system of the perturbation velocity vector, viz, $(u, v, w) = (\text{fluid velocity} - \vec{U}$
$\vec{U}$ = simulated freestream vector
U = magnitude of $\vec{U}$
v_t = tangential (to S) component of (u,v,w)
v_n = normal (to S) component of (u,v,w)
$V_{n_{ij}}$, $V_{t_{ij}}$ = matrices giving v_n and v_t, respectively, at point i due to unit increase of strength of jth panel, including indirect effect due to model
x,y,z = Cartesian coordinate system (Fig. 1); the x direction is parallel to the tunnel axis
α = angle of attack
Γ = circulation; thus Γ_r = strength of rth dipole panel of the jet-flap model
$\delta f, \delta v_n$ = mismatch signal defined in Table 1, step 4
Δq = increment in source strength q (see Table 5)
θ = inclination of wake panel relative to tunnel axis
Σ = surface formed by wall-control panels, "the tunnel wall"

Subscripts

G = point G, the midpoint of the transverse vortex segment of a plane horseshoe vortex
i = field-point number (point on S)
j = panel number (panel on Σ)
n = normal
r = panel number (panel of wing/wake model)
t = tangential

Superscript

(p) = quantities pertaining to the pth iteration

Presented as Paper 82-0541 at the ICAS/AIAA Aircraft Systems and Technology Meeting, Seattle, Wash., Aug. 22-27, 1982; submitted Aug. 30, 1982; revision received May 5, 1983.

*Professor. Honorary Fellow AIAA.

I. Introduction

THE special problem posed by the wind tunnel testing of V/STOL configurations is that they produce very large lift coefficients and, therefore, large deflections of the airstream. Thus, whereas the regime of flight at very low forward speeds—the "transition" regime—is typically the most important in the wind tunnel schedule, it is also the one exhibiting the greatest flow deflections and posing the most serious problems for the wind tunnel operator. Testing in this regime requires accurate simulation of energized, vortical wakes that are strongly directed downward and are often grossly distorted by the tunnel boundaries, including the floor.

The present paper reports studies carried out at the University of Arizona, under sponsorship of the U.S. Office of Naval Research, intended to solve this problem by exploitation of the concept of adaptive wind tunnel walls.

We begin with a short review of this concept and argue that it eliminates, along with boundary interference, the inaccuracies of the usual tunnel calibration. We then proceed to describe some numerical models of adaptive-wall tunnels, showing, in particular, that the undisturbed-stream direction and magnitude, arbitrarily chosen, are achieved by the iterative process of such a tunnel.

The evidence resulting from these simulations leads to a new idea in V/STOL testing in which flow geometry is chosen to obviate the problem of the wake, and the simulated stream direction is divorced from the architecture of the tunnel and attained by the adaptive-wall strategy.

Next, to demonstrate the use of this type of tunnel in an extreme case, a numerical model of a representative powered-lift wing in a strongly nonlinear regime is needed. An approximate panel representation of a jet-flap wing of finite span is therefore constructed. Finally, the testing of such a wing in this kind of tunnel is modeled; i.e., the iterative process by which this wing is brought from an arbitrary initial situation to the desired unconfined-flow condition is simulated in detail. This demonstration, while somewhat

tedious, is completely successful suggesting that the new tunnel would solve the recurring problem of V/STOL testing.

II. The Adaptive-Wall Concept

The idea of a wind tunnel whose working section walls are modified during each experiment so as to produce, for whatever configuration may be under test, an exact simulation of flight conditions originated in the early 1970s,[1,2] has been discussed for some years now, and would not seem to require detailed presentation in this paper. Nevertheless, a brief summary may be helpful to readers.

The scheme requires a) that the working-section walls be provided with control organs such that their shape, porosity, and/or exterior plenum pressures can be modified, and b) that instrumentation be provided within the working section to measure certain flow variables with the model in place. This instrumentation defines a surface S surrounding the model and measures the required flow variables at (in principle) all points of S. The wall-control organs must be capable of controlling flow conditions on S and are iteratively adjusted to produce unconfined-flow conditions there.

The third necessary feature of an adaptable-wall tunnel is c) capability to calculate the flowfield external to S; i.e., computing hardware and software to model numerically, for given boundary data on S, this external flowfield including its appropriate far-field boundary conditions. The surface S is therefore the *interface* between the flowfield actually produced inside S with model in place, engines running, etc., and the calculated exterior flowfield that satisfies the far-field conditions but, of course, exists only within the computer.

In practice, the adjustment to unconfined flow is accomplished as follows:

1) Two flow variables, say $f^{(1)}$ and $g^{(1)}$, are measured on S. Clearly, these are either consistent with the required far-field conditions, or they are not. In other words, either of these measured functions is adequate, together with far-field conditions, to define an exterior flowfield; in this sense the other measured function is redundant.

2) One of these functions, say $f^{(1)}$, is used as boundary data on S and the corresponding external field is calculated, satisfying far-field conditions. The other variable, say $g[f^{(1)}]$, is read out from this calculation and is compared with the measured function $g^{(1)}$. The difference $g[f^{(1)}] - g^{(1)}$, which we call $\delta^{(1)}g$, measures the degree of mismatch at the interface.

3) The wall-control organs are adjusted so as to add a fraction of $\delta^{(1)}g$, say $k\delta^{(1)}g$, where $0<k<1$, to the previously measured values $g^{(1)}$ on S. New distributions $f^{(2)}$ and $g^{(2)}$, presumably improved, are measured, the computations in step 2 are repeated, and so on until the function δg is as small as desired, or as small as can be achieved in a given experiment. If δg is zero, the inner and outer flows match on S and the matched flow satisfies all the boundary conditions; the flow in the tunnel is a correct representation of unconfined flow. This process is summarized in Table 1.

The adaptive-wall scheme has now been demonstrated successfully, both in real wind tunnels and in numerical simulation, in a number of laboratories, principally in the regime of transonic flow speeds.[3,4]

Table 1 Outline of the adaptable-wall iteration

1) Set model configuration (α, flap angles, power, etc.) and initial tunnel configuration (arbitrary).
2) Measure $f^{(1)}$ and $g^{(1)}$ on interface S.
3) Calculate outer flowfield with $f^{(1)}$ as boundary values and read out $g[f^{(1)}]$.
4) Form $\delta^{(1)}g = g[f^{(1)}] - g^{(1)}$ and $g^{(2)} = g^{(1)} + k\delta^{(1)}g$.
5) Adjust wall-control organs to obtain $g = g^{(2)}$ on S.
6) Repeat from step 2: ($g^{(n+1)} = g^{(n)} + k\delta^{(n)}g$, etc.) until $\delta^{(n)}g$ is as small as required.

III. Determination of Freestream Vector

In these studies and experiments, emphasis typically has been put on elimination of wall interference and not on questions of tunnel calibration. It has not always been appreciated that the adaptive-wall technique essentially eliminates the need for speed calibration and also removes the possibility of errors in the "undisturbed-flow direction."

Errors in both the speed calibration and the simulated undisturbed-flow direction are probably present in most wind tunnels when large and/or high-lift models are tested. The undisturbed stream vector $\vec{U}$ is a fictitious value that does not actually occur anywhere in a typical wind tunnel test. According to the tunnel's speed-calibration curves, the flow speed U would obtain in the empty working section if the appropriate manometer pressure difference were maintained. The effect of the model on this calibration is not usually known, but is assumed to be small. Regarding the simulated flow direction, the situation is even more uncertain: care is taken to assure that the empty-tunnel flow is accurately parallel to the drag direction of the balance system, e.g., horizontal, but there is little reason to believe that the simulated vector $\vec{U}$ therefore has the same direction when a large model is being tested.

Unfortunately, it is of primary importance to know $\vec{U}$ accurately in both magnitude and direction. For example, since the force on a model is decomposed into lift and drag by the balances, any error in flow direction, arg $\vec{U}$, results in large errors in drag, specifically an error of the amount $L \cdot \Delta\theta$, where L is the lift and $\Delta\theta$ is the error in simulated flow direction. Thus, errors $\Delta\theta$ of about 0.1 deg (0.0017 rad) make significant errors in measured drag for many cruise configurations!

In an adaptive-wall tunnel the stream vector $\vec{U}$ is selected by the operator and put into the exterior-flow calculation. The process of iteration to unconfined flow then leads, in principle, to correct simulation in the tunnel at this stream magnitude and direction, provided only that the instrumentation (b above) and exterior-flow computation (c above) are sufficiently accurate and the wall-control mechanism (a above) is adequate to provide conditions demanded by the iterative algorithm.

To be sure, the need for high accuracy in the determination of the vector $\vec{U}$, pointed out here, probably pertains more to tests at long-range cruise conditions than to the high-lift, V/STOL transition regime that is the primary concern of this paper. Nevertheless, as will be shown, the ability of the tunnel operator to select $\vec{U}$ *at will* in an adaptive-wall tunnel is essential in solving the V/STOL problem.

IV. Numerical Studies of V/STOL Wind Tunnels

Studies by the author at the University of Arizona have involved simulation, by panel methods, of incompressible flow about lifting wings in rectangular working sections. It may be useful to remind the reader at this point that "numerical simulation" here means that the processes of flow modification by means of wall elements and of measurement of flow properties on S are modeled numerically, while the calculation of exterior flow and the process of iteration are carried out exactly as they would be in practice if the tunnel existed. Of course, a wing and its response to flow in the tunnel must also be modeled.

In view of the large flow deflection expected, it was believed necessary to use an interface S that enclosed the wing and to control flow conditions at its upstream (and, perhaps, downstream) face. It will be recognized that the exterior-flow calculation, both in these simulations and in actual operation of a wind tunnel, would be greatly complicated by a wake emerging from S into the exterior-flow region. Early in the program, therefore, numerical experiments were carried out to resolve this matter. These confirmed that such a vortical wake did indeed make the calculation difficult, but that the

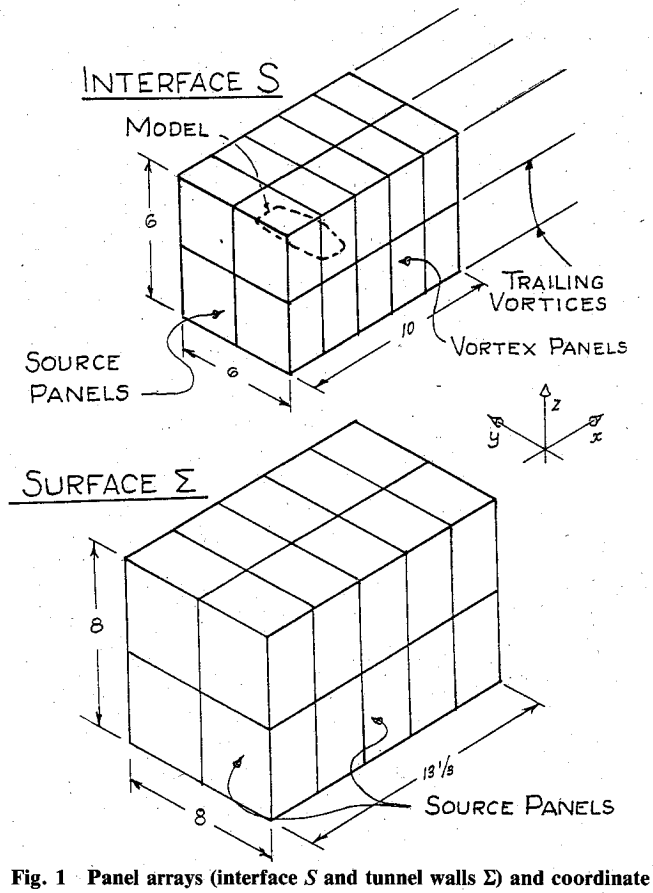

Fig. 1 Panel arrays (interface S and tunnel walls Σ) and coordinate system.

difficulties could be eliminated by extending the interface S downstream so far that the wake did not penetrate it.

The tunnel configuration thus arrived at is sketched in Fig. 1. In it, the interface S is square in cross section, closed upstream, and extends indefinitely downstream. For the exterior-flow calculation, the four sides of S are made up of rectangular panels of constant distributed-vortex strength. These are the singularity panels commonly used in aerodynamic studies, in which the transverse vortex strength (γ_y or γ_z) is uniform while γ_x is concentrated in line vortices at the lateral edges of the panels. Since these vortices extend indefinitely in the x direction, the interface can be said to be infinite in extent. The front face of S is made up of source panels of constant strength. There is a single measurement station ("field point") at the midpoint of each panel of S.

This semi-infinite interface S is enclosed in another, larger, rectangular array of uniform-source panels, Σ, as shown; this represents the array of control organs at the walls of a tunnel. Experience shows that flow conditions at the field points of S can be controlled to an adequate degree (as will be shown below) by this five-sided rectangular array. The two flow quantities f and g are chosen to be the tangential and normal components of the perturbation velocity vector, v_t and v_n. In terms of Cartesian components u,v,w, we take v_t to be w on the upstream face of S and u on the sides, top, and bottom; v_n, of course, is u on the upstream face, v on the sides, and w on top and bottom. (The panels of S and Σ were designed to be used with these choices for f and g.) As indicated in the Nomenclature, the perturbation vector is always defined relative to the specified, desired, freestream velocity vector.

Initial numerical experiments using arrays of this kind with various numbers of panels were made with a "responsive" horseshoe-vortex wing in the tunnel. This nomenclature denotes a horseshoe vortex lying in the xy plane whose circulation Γ is linearly related to the velocity components u and w at the midpoint of its transverse segment (point G). For

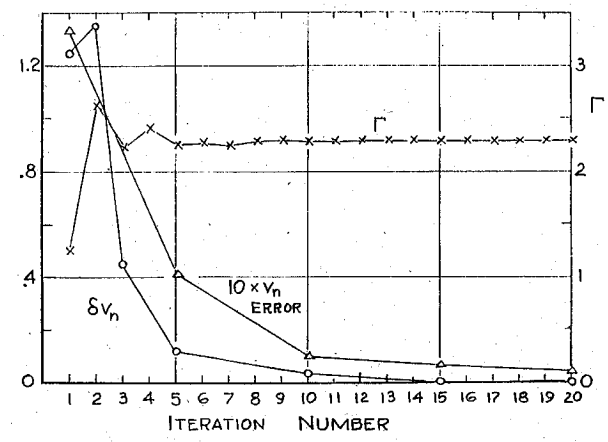

Fig. 2 Iteration of responsive horseshoe-vortex wing to unconfined flow in wind tunnel, $k=0.25$. Initial condition: $\vec{U}=0.8$ at zero inclination, with wall interference. Final condition: $\vec{U}=1.0$ at 0.25 rad, unconfined flow. ×, circulation Γ (right-hand scale); ○, maximum $|\delta v_n|$ on S (left-hand scale); Δ, average absolute true error in v_n on S (left-hand scale). (The points are connected only for clarity.)

example, if the stream vector is $\vec{U}=(1,0,0)$, we put

$$\Gamma=(\pi/2)\{1+u_G+2w_G\} \tag{1}$$

where u_G and w_G are perturbation velocity components, relative to $\vec{U}$, at point G. This can be interpreted as the circulation about a wing of unit chord whose effective incidence is 0.5 rad. The span of the horseshoe is four units, which is half of the width and height of Σ.

With this very simple wing model, the adaptive-wall process was carried out for a variety of initial conditions including wall interference (extraneous velocity perturbations) and errors in $\vec{U}$, using various arrangements of panels on S and Σ, and various values of the relaxation factor k.

An essential step in this modeling (as it is in real operation of an adaptive tunnel) is to determine the strengths of the panels of Σ, representing the setting of wall-control organs, to change the flow variable g (viz, v_n) at S by the chosen amount $k\delta g$ in any given iteration. Now, for incompressible irrotational flow and a linear wing model, the values of v_n are linearly related to the source strengths of Σ panels; the calculation is therefore a simple inversion of the matrix that expresses the influence of the Σ panels on v_n at field points of S. But the matrix must include both the direct influence of the Σ panels at the field points and the indirect effect; namely, the effects at the field points caused by the effects of Σ panels on the wing, i.e., on its circulation. We call this the "combined matrix." Similarly, of course, the values of f (viz, v_t) that result from the adjustment of Σ-panel strengths must also be calculated by means of a combined v_t matrix.

When the number of panels on Σ is the same as the number of field points on S, these calculations involve square matrices and are straightforward. It is desirable, however, to have more field points than Σ panels; in this case the source strengths on Σ are determined by a least-square-error procedure that gives a best fit to the updated v_n vector.

Figure 2 presents a typical result of these studies; namely, the results of a run made to demonstrate the ability of this model tunnel to produce an arbitrarily selected stream vector $\vec{U}$. The desired stream vector was chosen to be of unit magnitude at an angle of 0.25 rad to the x axis. The initial condition, as indicated, was assumed to involve an erroneous stream vector as well as conventional wall interference, represented here by "image" horseshoe vortices reflected in the tunnel walls. As indicated above, the arrays Σ and S are again aligned with the x axis; the horseshoe-vortex wing also lies in the xy plane. For Γ, Eq. (1) was modified appropriately for this calculation, since the unconfined flow now involves a

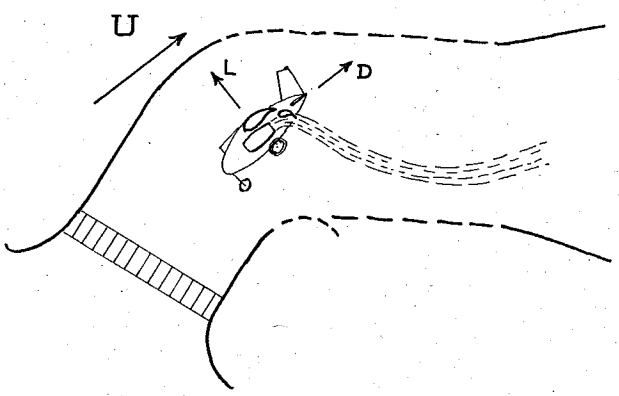

Fig. 3 Sketch of a proposed wind tunnel of the AVT type.

different stream vector; the unconfined-flow value of Γ for this case is 2.30 in the units used here.

As Fig. 2 shows, convergence to unconfined flow at the desired stream condition was obtained. Three quantities are plotted against the iteration number: 1) the circulation Γ, 2) the maximum value of $|\delta v_n|$ on S, and 3) the absolute true error in v_n averaged over the field points of S. This third quantity, the "true error," may require some explanation: In this particular case the exact flowfield of the horseshoe-vortex wing with circulation 2.30 is, of course, known. The converged values of v_n at the field points of S can therefore be compared with these exact values and the absolute error evaluated. It is clearly not the same as δv_n, since δv_n is the difference between inner and outer flows, both modeled by rather crude numerical methods. If δv_n were exactly zero, this true error would still not necessarily vanish, and would measure the ultimate ability of the chosen Σ-panel array to simulate unconfined horseshoe-vortex flow.

The value of k, the relaxation constant, was 0.25 in this run. As predicted above, there is measurable error in the final, converged flowfield, as indicated by the average "true error," but it is less than 1% of the stream speed. Figure 2 is typical of many trials made with the "responsive horseshoe-vortex" wing with various initial conditions, especially errors in stream magnitude and/or direction and various final conditions.

V. The Arizona V/STOL Wind Tunnel

At this point we have presented evidence suggesting 1) that the adaptive-wall scheme permits the stream direction and magnitude to be chosen independently of the geometry of the wind tunnel and 2) that the difficulties posed by the wake can be avoided if the wake does not emerge from the interface S. Together, these conclusions lead to the concept of a new kind of wind tunnel, in which model attitude is chosen to conform to paint 2 and simulated stream direction is then chosen to produce the desired angle of attack as in paint 1. This constitutes the Arizona V/STOL Tunnel (AVT).

Since our objective is to accommodate cases where the wake is grossly deflected from the stream direction, and since the interface must lie within the tunnel, it seems clear that the architecture of the tunnel must be divorced from the stream direction. In particular, there must be provision for strong vertical crossflow in the tunnel up- and downstream of the model. A rough, conceptual sketch of an AVT is presented in Fig. 3. We presume that a variable-angle nozzle upstream would provide the conditions required there without excessive turbulence. The nozzle angle would constitute one of the control organs of the adaptable-wall scheme, as would the tunnel's speed control. We assume that the conditions required downstream of the model can best be achieved by control of wall porosity and/or pressure in subdivided plenum chambers, and that turbulence may be less critical here than upstream.

Table 2 Outline of AVT procedure

1) Set model configuration: flap angles, power, etc.
2) Set initial tunnel configuration and approximate speed.
3) Rotate model so that wake trails downstream without impinging on instrumentation defining S.
4) Choose stream vector $\vec{U}$ to give desired angle of attack, and begin iteration to unconfined flow, as outlined in Table 1.
5) If wake changes position sufficiently to interfere with S, rotate model and stream vector equal amounts and proceed with iteration.

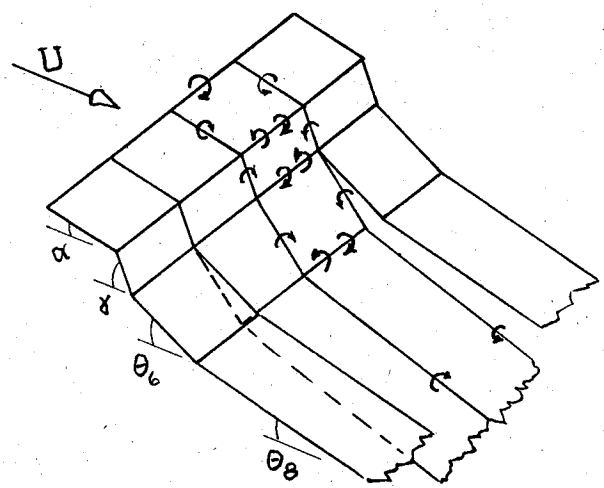

Fig. 4 Sketch showing panel model of jet-flap wing and wake.

In any case, the operating procedure for this type of tunnel will be unlike that of conventional tunnels. To run a test at a given angle of attack α, it will be necessary to guess at a freestream direction and model orientation, their difference being α, that will put the wake properly within S. (It should be easy to provide simple total-head or pitot-static tubes to ascertain roughly the wake position.)

To be sure, the wake position is affected by all other variables and may change during adjustment of the adaptable walls. The sequence of events appears to be that outlined in Table 2.

The next objective of this investigation is to demonstrate, by numerical simulation, that a tunnel of the AVT category can, in fact, be brought to unconfined-flow conditions with a powered-lift model in place at a large lift coefficient. For this purpose, a rectangular tunnel model similar to the one described and used above will be employed, but it is necessary to provide a simple, suitable, high-lift wing model as well.

VI. A Simple Jet-Flap-Wing Model

The jet-flap wing is an attractive example since it can be modeled rather simply. Its theory has been presented in Refs. 5-8. A numerical representation suitable for nonlinear, large-deflection cases is given in Ref. 9, and a panel method for high-lift conventional wings is given in Ref. 10.

Here we use the array of dipole panels (rectangular vortex rings) sketched in Fig. 4. There are 16 panels of constant dipole strength; 8 represent the wing and its mechanical flap and therefore have specified angles of incidence; the remaining 8 represent the momentum wake, whose shape is unknown and must be determined.

Two wake conditions determine this shape:

I) The wake is impermeable; thus the total normal velocity component—here evaluated at a single selected field point on each panel—must vanish.

II) The normal force on the wake is proportional to the jet momentum flux and the wake curvature.

In the present approximation, wake circulation is concentrated in vortex filaments at the lines where the panels join. The force is therefore concentrated there too, and produces finite angular deflections there. We neglect the lateral velocity components at the wake panels; they also affect the wake shape, but the vertical deflection of the wake is much larger near the wing and, therefore, more important.

It will be recognized that the unknowns here are the 16 panel strengths Γ_r and 8 wake-panel angles θ_r. These are determined by 16 kinematic conditions (I, above) and 8 force conditions (II). For large deflections (high lift), these relations are nonlinear. We obtain a solution for a given wing and given jet-momentum flux by assuming that the changes of wake deflections from one iteration to the next are small angles; this permits linearization of the trigonometric functions involved.

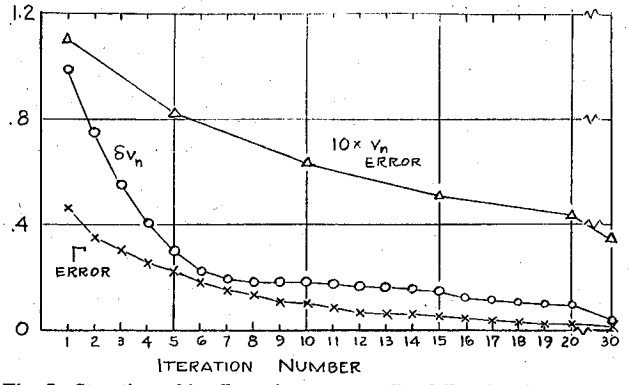

Fig. 5 Iteration of jet-flap wing to unconfined flow in wind tunnel, $k = 0.05$. 28 Σ panels, 28 points on S. Initial condition: $\bar{U} = 1.0$ at 45 deg ($\alpha = 0$ deg). Final condition: $\bar{U} = 1.0$ at 60 deg ($\alpha = 15$ deg). ×, average absolute error in Γ_r; ○, maximum $|\delta v_n|$ on S; Δ, average absolute true error in v_n on S. (The points are connected only for clarity.) $C = 0.5$.

Table 3 Definition of case simulated

Wing span	4.0
Wing chord including flap	1.2
Flap angle relative to wing	60 deg
Jet-momentum coefficient	$C = 0.5$
Desired angle of attack	$\alpha = 15$ deg
Desired stream speed	$U = 1.0$
Wing angle relative to tunnel axis	−45 deg

Note: From the above data it follows that the simulated stream vector $\bar{U}$ should make an angle of 60 deg to the tunnel axis.

Other quantities involved in conditions I and II are flowfield quantities and are evaluated from the preceding iteration. In other words, the solution is obtained by local linearization at each step, assuming small change of wake deflection in the next step. This technique requires that a guess be made for the θ_r to get the process started. The calculation at each step is then the solution of a set of linear algebraic equations for which rapid matrix techniques are available.

Before this model was used in our wind tunnel studies, it was exercised in cases of unconfined flow at various angles of attack and jet-momentum coefficients. The Cyber 175 computer at the University of Arizona was used. The effects of increasing the number of panels, both laterally and longitudinally, were also investigated. It was found that 10-15 iterations were required to reach convergence in unconfined flow. In the interest of brevity, further details concerning the jet-flap-wing model will not be presented here; interested readers are referred to Ref. 11.

VII. Simulation of a Test of the Jet-Flap Wing in the AVT

We now propose to demonstrate that a tunnel of the AVT type can be used to produce unconfined conditions around a jet-flap wing of the kind just described, at very large lift coefficients and large wake deflections, when the initial conditions are far from those desired. As already mentioned, the tunnel is modeled by a rectangular panel array similar to that used previously. Thus, although we have in mind a tunnel like the one sketched in Fig. 3, for example, we do not attempt to model its upstream geometry in detail. Rather, we assume that the rectangular panel arrays, Σ and S of Fig. 1, represent a category of AVT tunnels having instrumentation to measure v_n and v_t on the open-ended interface S and having wall-control organs capable of performing the equivalent of the functions of the source panels of Σ. The latter is, of course, a strong assumption; it means that we are testing here the principles of the AVT but not, so far as concerns wall-control organs, detailed features.

The panel arrays used here differ from Fig. 1 only in number, as follows: Top and bottom faces: 8 panels each; sides: 4 panels each; and front: 4 panels (as in Fig. 1). Thus, there are 28 Σ panels and 28 field points on S.

The numerical demonstration simulates an experimental case in which the jet-flap wing with given flap angle and jet coefficient is placed in the tunnel and the tunnel started up, but at a grossly wrong freestream angle. We assume that the energized wake lies properly within S—in other words, the model's attitude in the tunnel has been adjusted to place the

Table 4 Outline of numerical simulation of jet-flap wing in AVT

For given model configuration α, C, etc., and freestream vector $\bar{U}$:

1) Arbitrary starting situation in chosen (e.g., unconfined flow at wrong $\bar{U}$). Perturbation components $v_n^{(1)}$ and $v_t^{(1)}$ on interface are calculated [e.g., by iterating wing program for unconfined flow ($q_j^{(1)} = 0$)]. *This is wing configuration 1.*
2) Outer flow is calculated: viz, v_n [$v_t^{(1)}$] and $\delta^{(1)} v_n$.
3) "Combined" influence matrices $V_{nij}^{(1)}$ and $V_{tij}^{(1)}$ and $q_j^{(2)}$ are calculated as follows (linearization about wing configuration 1):
   a) With $q_j = q_j^{(1)} + (0.01,0,0,\ldots)$ the wing is iterated. $V_{ni1}^{(1)}$ and $V_{ti1}^{(1)}$ are obtained, including "direct" effects of q_j.
   b) With $q_j = q_j^{(1)} + (0,0.01,0,\ldots)$ the wing is iterated. $V_{ni2}^{(1)}$ and $V_{ti2}^{(1)}$ are obtained, including "direct" effects of q_j, etc.
   c) $V_{nij}^{(1)} \Delta^{(1)} q_j = k\delta^{(1)} v_{ni}$ is solved for $\Delta^{(1)} q_j$.
4) With $q_j = q_j^{(2)} = q_j^{(1)} + \Delta^{(1)} q_j$ the wing is iterated yielding *wing configuration 2.*
5) Inner flow is calculated; viz, $v_n^{(2)}$ and $v_t^{(2)}$ for wing configuration 2 and $q_j = q_j^{(2)}$.
6) Step 2 is repeated yielding v_n [$v_t^{(2)}$] and $\delta^{(2)} v_n$.
7) Step 3 is repeated yielding new matrices $V_{nij}^{(2)}$ and $V_{tij}^{(2)}$ and $q_j^{(3)}$ (linearization about wing configuration 2):
   a) With $q_j = q_j^{(2)} + (0.01,0,0,\ldots)$ the wing is iterated. $V_{ni1}^{(2)}$ and $V_{ti1}^{(2)}$ are obtained, including "direct" effects of q_j.
   b) With $q_j = q_j^{(2)} + (0,0.01,0,\ldots)$ the wing is iterated. $V_{ni2}^{(2)}$ and $V_{ti2}^{(1)}$ are obtained, including "direct" effects of q_j, etc.
   c) $V_{nij}^{(2)} \Delta^{(2)} q_j = k\delta^{(2)} v_n$ is solved for $\Delta^{(2)} q_j$.
8) With $q_j = q_j^{(3)} = q_j^{(2)} + \Delta^{(2)} q_j$ the wing is iterated yielding *wing configuration 3.*
9) Step 5 is repeated, yielding $v_n^{(3)}$ and $v_t^{(3)}$ for wing configuration 3 and $q_j = q_j^{(3)}$.

Etc. to convergence.

Table 5 Results of iteration of jet-flap wing to unconfined flow in wind tunnel[a]

Iteration No.	Γ_1	Γ_2	Γ_3	Γ_4	Γ_5	Γ_6	Γ_7	Γ_8	θ_5, deg	θ_6, deg	θ_7, deg	θ_8, deg
1	1.26	0.96	2.15	1.75	2.31	1.88	2.38	1.94	0.92	3.97	−5.93	0
3	1.44	1.11	2.33	1.90	2.49	2.03	2.57	2.08	1.00	4.26	−5.71	0.73
6	1.60	1.25	2.50	2.03	2.66	2.17	2.74	2.22	1.07	4.57	−5.48	1.48
10	1.70	1.33	2.60	2.12	2.77	2.26	2.85	2.30	1.19	4.84	−5.20	2.09
15	1.77	1.39	2.66	2.16	2.83	2.30	2.92	2.35	1.30	5.04	−4.97	2.52
20	1.80	1.41	2.69	2.18	2.86	2.33	2.95	2.37	1.36	5.16	−4.84	2.74
30	1.82	1.43	2.72	2.20	2.89	2.34	2.97	2.39	1.40	5.24	−4.73	2.92
Unconfined	1.86	1.46	2.73	2.20	2.90	2.34	2.98	2.37	2.18	6.02	−3.31	4.59

[a] $K=0.05$. Initial condition: $\bar{U}=1.0$ at 45 deg ($\alpha=0$ deg). Initial condition: $\bar{U}=1.0$ at 60 deg ($\alpha=15$ deg). 28 Σ panels, 28 S paints, wing centered in tunnel. $C=0.5$.

wake there as in step 3 of Table 2. The simulated stream vector $\bar{U}$ is then chosen to produce the desired angle of attack, and the process of iteration is begun (see step 4 of Table 2).

The jet-flap-wing model of Sec. VI is well suited to this simulation. We begin with a freestream vector quite different from the desired $\bar{U}$ and use our jet-flap model to give us the resulting initial wing/wake configuration and flowfield. Adopting the adaptive-wall strategy, the wall panels are activated in accordance with the algorithm (Table 1). Our jet-flap model is then exercised again, this time in the presence of perturbations from the wall panels, leading to a new wing/wake configuration, and so on. If the procedure converges ($\delta v_n \to 0$), the perturbations due to wall panels are just those that cancel the errors of the initial situation, causing inner and outer fields to match at S. The outer field, it will be recalled, always satisfies the right conditions at infinity, viz, undisturbed flow at velocity $\bar{U}$. The wing/wake geometry and circulation distribution should then agree with unconfined-flow results for the same wing at the same values of α, $\bar{U}$, and C.

Table 3 presents data taken from a typical numerical case carried through in our studies; this case constitutes the numerical demonstration for the present paper.

Since the starting condition assumed to exist at step 4 of Table 2 is quite arbitrary, let us assume for this demonstration that the wing finds itself in conditions equal to unconfined flow at $U=1.0$ but at an angle of attack of 0 deg. In other words, at this point the tunnel has inadvertently been set in such a way as to simulate a freestream vector whose angle to the tunnel axis is 45 deg instead of the required 60 deg.

The jet-flap-wing model of Sec. VI of this paper was used, with $\alpha=0$ deg, to provide the wake geometry and circulation distribution corresponding to these initial conditions. This is called "wing/wake configuration 1." From these data we calculate v_n and v_t at the field points of S; these constitute the initial measured values of the experiment, designated $v_n^{(1)}$ and $v_t^{(1)}$. With these measured $v_t^{(1)}$ as boundary values, we calculate the exterior flow, specifically $v_n[v_t^{(1)}]$, and form $\delta^{(1)}v_n$. Next, choosing (by experience) a suitable value of the relaxation factor k (here we choose 0.05) we form the first improved values of v_n, viz,

$$v_n^{(2)} = v_n^{(1)} + k\delta^{(1)}v_n \tag{2}$$

These outer-flow calculations are exactly the same as would be carried out if the wind tunnel actually existed. Next, it would be necessary to adjust the wall-control organs in such a way as to produce these velocities $v_n^{(2)}$ at the field points of S. The way to do this probably would be to measure the influence matrix, say $V_{ij}^{(1)}$, giving the effects on v_n at i due to unit changes of the jth control organs. This could be done by making a small change in the setting of each control organ and measuring the resulting changes of v_{ni}.

Our procedure, for this numerical demonstration, is to simulate this process exactly: we evaluate the combined matrix $V_{ij}^{(1)}$. This requires that the strength of q_j of each source panel of Σ be increased slightly, one at a time, the jet-flap wing be iterated to convergence with consideration of the resulting velocity increments at the wing and wake panels, and the resulting "combined" increments in v_{ni} on S be calculated.

We can now invert $V_{ij}^{(1)}$ and calculate the total changes of source strengths q_j to produce the increments $k\delta^{(1)}v_n$ on S. In view of the nonlinearity, the calculated matrix pertains only to wing/wake configuration 1. We do not assume that our new q_j will produce exactly the v_n distribution of Eq. (2) when all panels are simultaneously adjusted; hence we actually re-iterate the jet-flap wing in the presence of the velocity field of all of our Σ panels together. The result is wing/wake configuration 2. Its geometry and circulation distribution now provide the values $v_{ni}^{(2)}$ and $v_{ti}^{(2)}$. (The $v_n^{(2)}$ calculated in Eq. (2) are not used further.) We are now ready for the second iteration.

It will be clear to the reader that each step of the iteration of the wind tunnel toward unconfined flow involves $N+1$ iterative calculations of jet-flap wing properties, where N is the number of wall-control panels. This numerical simulation is therefore a rather complex one, and may be clarified by an outline of steps, as presented in Table 4.

Again the Cyber 175 of the University of Arizona was used. Each "experiment" in this case required about 20 iterations in the adaptive-wall procedure. Since there were 28 Σ panels and lateral symmetry was assumed, the process of "experimentally" determining each member of the combined v_n matrix, described above, had to be carried out 14 times in each of these iteration steps; thus, 15 determinations of wing geometry and flowfield were made in each iteration step. Each of these determinations required at least 7 iterations of the wing geometry. Nevertheless, a typical "experiment" was carried out, from arbitrary starting situation to unconfined flow, in about a minute of computer time.

Results of this calculation are presented in Fig. 5 and Table 5. In Fig. 5 are plotted 1) the mean absolute error in $\Gamma_i^{(p)}$, 2) the maximum absolute value of the "mismatch signal" $\delta^{(p)}v_n$ on S, and 3) the average absolute error in $v_n^{(p)}$ on S. The abscissa is the iteration number p. As has already been mentioned in connection with Fig. 2, the errors in paints 1 and 3 can be evaluated at any step of the iteration in this test case because the properties and flowfield of the jet-flap wing in unconfined flow are known.

It will be noted that the circulations of the various wing and wake panels, including the total lift (approximately proportional to the mean of Γ_7 and Γ_8 in this case), converge rapidly to a close approximation to unconfined-flow values. This means that the aerodynamic properties of the wing are accurately rendered. This occurs in spite of the rather slow convergence of δv_n toward zero and the persistence of an appreciable error in the flowfield at interface S.

VIII. Additional Simulations

Following this successful simulation of the jet-flap-wing model, a number of additional, related, numerical experiments were carried out; some of which will be summarized briefly here.

Mean-Square Fitting

The tunnel model employed in Sec. VII had 28 wall-control panels and 28 instrument locations (field points), as mentioned. Simulations were also carried out using the same array of 28 Σ panels (wall-control panels) together with 44 field points on S, as in Fig. 1. When the number of field points (say 44) exceeds the number of Σ panels (say 28); the 28 panel strengths q are made to fit the 44 boundary values v_n in a best-mean-square sense. Thus, it would be expected that the iteration procedure would lead to a better approximation to unconfined flow than given by a 28×28 model (but perhaps poorer than 44×44), and this improvement of results was indeed observed.

A larger k was used here than in Table 5; this was found to be possible when mean-square fitting was used. Runs were made with this (44×28) array with k equal to 0.15, 0.2, and 0.3. Most rapid convergence seemed to occur with $k=0.3$. Slightly more accurate results, as measured by the average absolute error of Γ_r, occurred with $k=0.20$.

Variable k

The use of a relaxation factor k that is uniform in space and also constant during the process of iteration is quite arbitrary. Various guesses have been made during this research as to what changes of k might accelerate convergence and/or improve final results. Our conclusion has been, to date, that convergence is accelerated if k is increased as the iteration is carried out. For example, in one run, k was put equal to 0.10 for the first 10 iterations, then increased by 0.01 in each subsequent iteration to a value of 0.20 in the 20th step. The process converged appreciably faster than with $k=0.10$, 0.15, or 0.20.

Model with Horizontal Tail Surface

Runs were also made in which a typical horizontal tail surface was modeled together with the wing. This surface was modeled as a simple horseshoe vortex carrying a download, located one-half span behind the wing. The tail span was chosen to be half that of the wing. The circulation of this horseshoe vortex was determined by the total perturbation velocity at the tail position. The horizontal tail had only minor effects on $\Gamma_1,\ldots,\Gamma_8$ and the wake configuration.

Changes of Wing Location and Stream Inclination

It will be recalled that the central idea of the AVT is to place the wake so that it does not impinge on either tunnel boundaries (Σ) or instrument array (S). Clearly, this can be accomplished in a variety of ways: there is a range of stream inclinations (arg $\vec{U}$) within which the wake, for any wing configuration, lies somewhere between the top and bottom surfaces of the interface S as it leaves the working section downstream. This range can be increased by placing the model higher in the tunnel. It is interesting to ask whether changes of stream inclination and/or model position make any difference in the converged results obtained. Runs were made to explore these questions. The wing-plus-tail model was employed in these simulations. Only very small changes resulted. We take this to mean that model height can be maximized and stream inclination minimized in order to accommodate cases of extreme wake deflection without impairing the accuracy of the tunnel.

IX. Concluding Remarks

On the basis of the numerical simulations reported here, it appears that a tunnel of AVT type can be used to test high-lift configurations, correcting for gross errors in starting conditions and arriving at conditions closely approximating unconfined flow. Since the simulations carried out make no pretense of modeling in detail the properties of real wall-control organs, no further conclusions can be drawn until the program is moved from the realm of numerical simulation into the realm of laboratory experiments. Work now proceeds toward the construction and testing of a demonstration version of the AVT.

Acknowledgments

This project has been supported at the University of Arizona, Department of Aerospace and Mechanical Engineering, by Contract N 00014-79-C-0010. The encouragement, as well as invaluable technical advice, received from Morton Cooper is gratefully acknowledged. The author also acknowledges the able assistance of Karl Allmendinger and Daniel C.L. Lee, graduate assistants at the University of Arizona.

References

[1] Ferri, A. and Baronti, P., "A Method for Transonic Wind Tunnel Corrections," *AIAA Journal*, Vol. 11, Jan. 1973, pp. 63-66.

[2] Sears, W.R., "Self-Correcting Wind Tunnels," *Aeronautical Journal*, Vol. 78, Feb./March 1974, pp. 80-89.

[3] Sears, W.R., Vidal, R.J., Erickson, J.C. Jr., and Ritter, A., "Interference-Free Wind-Tunnel Flows by Adaptive-Wall Technology," *Journal of Aircraft*, Vol. 14, Nov. 1977, pp. 1042-1050.

[4] Satyanarayana, B., Schairer, E., and Davis, S., "Adaptive-Wall Wind-Tunnel Development for Transonic Testing," *Journal of Aircraft*, Vol. 18, April 1981, pp. 273-279.

[5] Spence, D.A. "The Lift Coefficient of a Thin, Jet-Flapped Wing," *Proceedings of the Royal Society*, Vol. A238, Dec. 1956, pp. 46-68.

[6] Maskell, E.C. and Spence, D.A., "A Theory of the Jet Flap in Three Dimensions," *Proceedings of the Royal Society*, Vol. A251, June 1959, pp. 407-425.

[7] Kerney, K.P., "An Asymptotic Theory of the High-Aspect-Ratio Jet Flap," Ph.D. Thesis, Graduate School of Aeronautical Engineering, Cornell University, Ithaca, N.Y. 1967.

[8] Tokuda, N., "An Asymptotic Theory of the Jet Flap in Three Dimensions," *Journal of Fluid Mechanics*, Vol. 46, Pt. 4, 1971, pp. 705-726.

[9] Addessio, F.L. and Shifstad, J.G., "Aerodynamics of a Finite Aspect Ratio Jet Flap at Low Flight Speeds," *Journal of Aircraft*, Vol. 14, Oct. 1977, pp. 936-943.

[10] Maskew, B., "A Quadrilateral Vortex Method Applied to Configurations with High Circulation," NASA SP-405, 1976, pp. 163-186.

[11] Lee, D.C.L., "The Modelling of a High-Lift Jet-Flapped Wing," Master of Science Report, Department of Aerospace and Mechanical Engineering, University of Arizona, Tucson, Ariz., 1981.